fractal and fractional

Article

Series with Binomial-like Coefficients for the Investigation of Fractal Structures Associated with the Riemann Zeta Function

Igoris Belovas *, Martynas Sabaliauskas and Lukas Kuzma

Institute of Data Science and Digital Technologies, Faculty of Mathematics and Informatics, Vilnius University, LT-04812 Vilnius, Lithuania; martynas.sabaliauskas@mif.vu.lt (M.S.); lukas.kuzma@mif.vu.lt (L.K.)
* Correspondence: igoris.belovas@mif.vu.lt

Abstract: The paper continues the study of efficient algorithms for the computation of zeta functions over the complex plane. We aim to apply the modifications of algorithms to the investigation of underlying fractal structures associated with the Riemann zeta function. We discuss the computational complexity and numerical aspects of the implemented algorithms based on series with binomial-like coefficients.

Keywords: Riemann zeta function; fractal structures; numerical algorithms

check for updates

Citation: Belovas, I.; Sabaliauskas, M.; Kuzma, L. Series with Binomial-like Coefficients for the Investigation of Fractal Structures Associated with the Riemann Zeta Function. *Fractal Fract.* **2022**, *6*, 300. https://doi.org/10.3390/fractalfract6060300

Academic Editor: Palle Jorgensen

Received: 10 April 2022
Accepted: 27 May 2022
Published: 29 May 2022

1. Introduction

In this paper, we continue the study of efficient algorithms for computation of the Riemann zeta function over the complex plane, introduced by Borwein [1] and extended by Belovas et al., (see [2,3] and references therein). Šleževičienė [4], Vepštas [5], and Coffey [6] applied this methodology for the computation of Dirichlet L-functions, Hurwitz zeta function, and polylogarithm. Belovas et al. obtained limit theorems, which allowed the introduction of asymptotic approximations for the coefficients of the series of the algorithms. A preliminary presentation of computational aspects of the approach has been presented in [3]. Theoretical aspects of the approach (as well as more subtle proofs of the limit theorems) have been discussed in [7].

Fractal geography of the Riemann zeta function (and other zeta functions) was addressed by King [8]. Woon [9] and Tingen [10] computed Julia and Mandelbrot sets of the Riemann zeta function and Hurwitz zeta function, respectively, and studied the properties of these fractals. Recently Blankers et al. [11] investigated the analogs of Julia and Mandelbrot sets for dynamical systems over the hyperbolic numbers. In the present study, we enhance algorithms for the calculation of the Riemann zeta function, proposed in [2,3]. We specify the convergence rate to the limiting distribution for the coefficients of the series, identify the error term, and discuss computational complexity. The algorithms are compared against the recently proposed *Zetafast* algorithm [12] and are applied for the investigation of underlying fractal structures associated with the Riemann zeta function.

The paper is organized as follows. The first part is the introduction. In Section 2, we describe algorithms and present theoretical results. Section 3 is devoted to the visual investigation of the underlying fractal background of the Riemann zeta function. Pseudocodes of the algorithms for the computation and the visualization are given in Section 4. Sections 5 and 6 are devoted to presenting the results and conclusions, respectively.

Throughout this paper, $U \times V$ stands for the Cartesian product of sets U and V. We denote by $\Phi(x)$ the cumulative distribution function of the standard normal distribution, and by $\Gamma(s)$ we denote the gamma function. Next, $\lfloor x \rfloor$ and $\lceil x \rceil$ stand for the floor function and the ceiling functions, respectively. All limits in the paper, unless specified, are taken as $n \to \infty$.

2. *MB*- and *BLC*-Algorithms for the Computation of the Riemann Zeta Function

Let $s = \sigma + it$ be a complex variable. The Riemann zeta-function is defined on the half-plane $\sigma > 1$ by the ordinary Dirichlet series or the Euler product formula,

$$\zeta(s) = \sum_{n=1}^{\infty} \frac{1}{n^s} = \prod_{p \text{ prime}} \left(1 - \frac{1}{p^s}\right)^{-1},$$

and by analytic continuation for other complex values. The Riemann zeta function is a meromorphic function (holomorphic on the whole complex plane except for a simple pole at $s = 1$ with residue 1). The Riemann zeta function satisfies the functional equation

$$\zeta(s) = 2^s \pi^{s-1} \sin(\pi s/2)\Gamma(1-s)\zeta(1-s),$$

implying that $\zeta(s)$ has simple zeros at $s = -2n$, $n \in \mathbb{N}$, known as the trivial zeros. Other zeroes are called nontrivial. The famous Riemann hypothesis states that all the nontrivial zeros lie on the critical line $s = 1/2 + it$. The hypothesis is closely related to the distribution of prime numbers, implying the best possible error term in the prime number theorem,

$$\pi(x) = \int_2^x \frac{dt}{\log t} + O(\sqrt{x} \log x).$$

Here $\pi(x)$ is the prime-counting function, i.e., the number of primes less than or equal to x , $x \in \mathbb{R}$. A summary of the literature covering the problems related to the Riemann zeta function and its applications is presented in [13,14] and the references therein.

2.1. MB-Algorithm

In [3] Belovas et al., proposed a modification of Borwein's efficient algorithm (*MB*-algorithm) for the computation of the Riemann zeta function [1]. The algorithm applies to complex numbers with $\sigma \geqslant 1/2$ and arbitrary t. The Riemann zeta function is represented by the alternating series

$$\zeta(s) = \frac{1}{1-2^{1-s}} \sum_{k=0}^{n-1} \frac{(-1)^k \psi_{n,k}^{(j)}}{(k+1)^s} + \gamma_n^{(j)}(s). \quad (1)$$

Here (case $j = 1$ in $\psi_{n,k}^{(j)}$ corresponds *MB*-series), by Theorem 1 from [3], we have

$$\psi_{n,k}^{(1)} = 1 - \frac{H_k}{H_n} \quad \text{and} \quad l_{max} = \arg \max_{0 \leqslant k \leqslant n} \frac{(n+k-1)!4^k}{(n-k)!(2k)!}, \quad n \in \mathbb{N}, \ 0 \leqslant k \leqslant n, \quad (2)$$

while

$$\begin{aligned} &H_l = H_{l-1} + \exp(T_l - T_{l_{max}} + (l - l_{max})\log 4), \quad &&H_0 = \exp(T_0 - T_{l_{max}} - l_{max}\log 4), \\ &T_l = T_{l-1} + \log\frac{(n-l+1)(n+l-1)}{(2l-1)(2l)}, &&T_0 = -\log n, \quad 1 \leqslant l \leqslant n. \end{aligned} \quad (3)$$

The algorithm is nearly optimal in the sense that there is no sequence of n-term exponential polynomials that converge to the Riemann zeta function much faster than of the algorithm (see Theorem 3.1 in [1]).

2.2. BLC-Algorithm

This algorithm, introduced in [2], also uses series (1) (case $j = 2$ in $\psi_{n,k}^{(j)}$ corresponds *BLC*-series), but with different binomial-like coefficients,

$$\psi_{n,k}^{(2)} = I_{1/2}(k+1, n-k+1). \quad (4)$$

Here $I_x(a,b)$ stands for the regularized incomplete beta function,

$$I_x(a,b) = \int_0^x t^{a-1}(1-t)^{b-1}dt \Big/ \int_0^1 t^{a-1}(1-t)^{b-1}dt.$$

The error terms $\gamma_n^{(j)}(s)$ of these methods are discussed in the following subsection.

2.3. Error Terms and Computational Complexity

First we formulate an auxiliary lemma, aiming to investigate the behaviour of the series in the neighbourhoods of critical points τ_k,

$$\tau_k = 1 + 2i\pi k/\log 2, \qquad k \in \mathbb{N}_0. \tag{5}$$

Note that in (1) the denominator $1 - 2^{1-s} = 0$ if and only if $\Im s = 2\pi k/\log 2$, $k \in \mathbb{Z}$ and $\Re s = 1$.

Lemma 1. *Let τ_k be defined by (5) and ω_k be the circle*

$$\omega_k = \{s : \ |s - \tau_k| = \rho > 0\}.$$

Then, for $f(s) = 1/(1 - 2^{1-s})$ and $\rho \leqslant 3/\log 2$,

$$\max_{s\in\omega_k} |f(s)| \leqslant \frac{1}{1-2^{-\rho}}. \tag{6}$$

Proof of Lemma 1. Parametrizing the complex function $f(s)$ for the circle ω_k, we obtain

$$g(\varphi) := f(\tau_k + \rho e^{i\varphi}) = 1/(\underbrace{1 - 2^{-2i\pi k/\log 2 - \rho(\cos\varphi + i\sin\varphi)}}_{:=u(\varphi)}). \tag{7}$$

Next,

$$\begin{aligned} |u(\varphi)| &= |1 - 2^{-\rho\cos\varphi}(\cos(\rho\log 2\sin\varphi) - i\sin(\rho\log 2\sin\varphi))| \\ &= (\underbrace{1 - 2^{1-\rho\cos\varphi}\cos(\rho\log 2\sin\varphi) + 2^{-2\rho\cos\varphi}}_{:=v(\varphi)})^{1/2}. \end{aligned} \tag{8}$$

The function $v(\varphi)$ is periodic with period 2π and symmetric with respect to $\varphi = \pi$ (indeed, $v(\pi - \chi) = v(\pi + \chi)$). Hence the statement of the lemma reduces to solving

$$\min_{0\leqslant\varphi\leqslant\pi} v(\varphi).$$

Differentiating $v(\varphi)$, we get for $0 < \varphi < \pi$

$$\begin{aligned} v'(\varphi) &= 2^{1-\rho\cos\varphi}\rho\log 2 \\ &\cdot \underbrace{(2^{-\rho\cos\varphi}\sin\varphi - \sin\varphi\cos(\rho\log 2\sin\varphi) + \cos\varphi\sin(\rho\log 2\sin\varphi))}_{:=w(\varphi)>0} > 0. \end{aligned}$$

Indeed, with $r = \rho\log 2$ and

1^0. $(r, \varphi) \in (0, 3) \times (0, \pi/2)$, we have

$$\begin{aligned} w(\varphi) &= e^{-r\cos\varphi}\sin\varphi - \sin\varphi\cos(r\sin\varphi) + \cos\varphi\sin(r\sin\varphi) \\ &\geqslant \left(1 - r\cos\varphi + \frac{1}{2}(r\cos\varphi)^2 - \frac{1}{6}(r\cos\varphi)^3\right)\sin\varphi \\ &- \left(1 - \frac{1}{2}(r\sin\varphi)^2 + \frac{1}{24}(r\sin\varphi)^4\right)\underbrace{\sin\varphi}_{>0} + \left(r\sin\varphi - \frac{1}{6}(r\sin\varphi)^3\right)\underbrace{\cos\varphi}_{>0} \\ &= \frac{1}{24}r^2\sin\varphi\left(12 - 4r\cos\varphi - r^2\sin^4\varphi\right) > 0. \end{aligned}$$

2^0. For $(r, \varphi) \in (0, 3) \times (\pi/2, \pi)$, we have

$$\begin{aligned} w(\varphi) &= e^{-r\cos\varphi}\sin\varphi - \sin\varphi\cos(r\sin\varphi) + \cos\varphi\sin(r\sin\varphi) \\ &\geqslant \left(1 - r\cos\varphi + \frac{1}{2}(r\cos\varphi)^2\right)\sin\varphi \\ &- \left(1 - \frac{1}{2}(r\sin\varphi)^2 + \frac{1}{24}(r\sin\varphi)^4\right)\underbrace{\sin\varphi}_{>0} + r\sin\varphi\underbrace{\cos\varphi}_{<0} \\ &= \frac{1}{24}r^2\sin\varphi\left(12 - r^2\sin^4\varphi\right) > 0. \end{aligned}$$

We have shown that $w(\varphi) > 0$ for $(r, \varphi) \in ((0, 3) \times (0, \pi/2)) \cup ((0, 3) \times (\pi/2, \pi))$. Note that $w(\pi/2) > 0$ for $r \in (0, 3)$. Thus the function $v(\varphi)$ is monotonically increasing and

$$v_{min} = \min_{0 \leqslant \varphi \leqslant \pi} v(\varphi) = v(0) = (1 - 2^{-\rho})^2,$$

with (7) and (8) yielding us the statement of the lemma. □

The error term and the computational complexity are closely linked to the problem of the selection of the minimal number of terms in the series (1). Let us formulate the following theorem.

Theorem 1. *Let $\sigma \geqslant 1/2$, $t \geqslant 0$, $\varepsilon > 0$ and $|s - \tau_k| \geqslant \varepsilon$, then*

(i) *the error term of the series* (1) *is*

$$|\gamma_n^{(j)}(s)| \leqslant \Theta_n^{(j)} \frac{(\cosh \pi t)^{1/2}}{|1 - 2^{1-s}|}, \tag{9}$$

(ii) *the series* (1) *to compute the Riemann zeta-function with d decimal digits of accuracy, require a number of terms*

$$n^{(j)} = \left\lceil D_1^{(j)} t + D_2^{(j)} d + D_\varepsilon^{(j)} \right\rceil, \tag{10}$$

with coefficients of expressions (9) *and* (10) *presented in Table 1.*

Table 1. Coefficients of expressions (9) and (10).

j	$\Theta_n^{(j)}$	$D_1^{(j)}$	$D_2^{(j)}$	$D_\varepsilon^{(j)}$
1	$\frac{2}{(3+\sqrt{8})^n}$	$\frac{\pi/2}{\log(3+\sqrt{8})}$	$\frac{\log 10}{\log(3+\sqrt{8})}$	$\frac{\log 2 - \log(1-2^{-\varepsilon})}{\log(3+\sqrt{8})}$
2	$\frac{1}{2^{n+1}}$	$\frac{\pi/2}{\log 2}$	$\frac{\log 10}{\log 2}$	$\frac{-\log 2 - \log(1-2^{-\varepsilon})}{\log 2}$

Proof of Theorem 1. Let us start with *MB*-series. The error term of the series (1) is (cf. Algorithm 2 in [1])

$$|\gamma_n^{(1)}(s)| \leqslant \frac{2}{(3+\sqrt{8})^n} \frac{1}{|1-2^{1-s}|} \frac{1}{|\Gamma(s)|} \underbrace{\int_0^1 \frac{(-\log x)^{\sigma-1}}{1+x} dx}_{:=I(\sigma)}. \tag{11}$$

Considering the function $I(\sigma)$, we have

$$I(\sigma) \leqslant \int_0^1 (-\log x)^{\sigma-1} dx = \Gamma(\sigma). \tag{12}$$

By a product representation of the gamma function (cf. 8.326.1 in [15]),

$$\left|\frac{\Gamma(\sigma)}{\Gamma(s)}\right|^2 = \prod_{n=0}^{\infty} \left(1 + \frac{t^2}{(\sigma+n)^2}\right),$$

The product is decreasing by σ, hence (cf. 8.332.2 in [15]),

$$\frac{\Gamma(\sigma)}{|\Gamma(s)|} \leqslant \frac{\Gamma(\frac{1}{2})}{|\Gamma(\frac{1}{2}+it)|} = \frac{\sqrt{\pi}}{\sqrt{\frac{\pi}{\cosh \pi t}}} = \sqrt{\cosh \pi t}. \tag{13}$$

Hence,

$$|\gamma_n^{(1)}(s)| \leqslant \frac{2}{(3+\sqrt{8})^n} \frac{\sqrt{\cosh \pi t}}{|1-2^{1-s}|}. \tag{14}$$

In view of (14), to compute the Riemann zeta-function with d decimal digits of accuracy, the approach requires a number n of terms not less than

$$\begin{aligned} N_d(\sigma,t) &= \frac{\log 2 + d\log 10 + \frac{1}{2}\log\cosh \pi t - \log|1-2^{1-s}|}{\log(3+\sqrt{8})} \\ &= \frac{\pi t + \log(1+e^{-2\pi t}) + \log 2 + 2d\log 10 - 2\log|1-2^{1-s}|}{2\log(3+\sqrt{8})} \\ &\leqslant \frac{\pi t + 2d\log 10 - 2\log|1-2^{1-s}| + 2\log 2}{2\log(3+\sqrt{8})}. \end{aligned} \tag{15}$$

1^0. Let $|\sigma-1| > \varepsilon$. We have

$$\begin{aligned} N_d(\sigma,t) &\leqslant \frac{\pi t + 2d\log 10 - 2\log|1-2^{1-\sigma}| + 2\log 2}{2\log(3+\sqrt{8})} \\ &\leqslant \frac{\pi/2}{\log(3+\sqrt{8})} t + \frac{\log 10}{\log(3+\sqrt{8})} d + \frac{\log 2 - \log(1-2^{-\varepsilon})}{\log(3+\sqrt{8})}. \end{aligned} \tag{16}$$

2^0. Let $|s-\tau_k| \geqslant \varepsilon$ and $|\sigma-1| \leqslant \varepsilon$. By applying the maximum modulus principle and Lemma 1, we receive

$$\begin{aligned} N_d(\sigma,t) &\leqslant \frac{\pi t + 2d\log 10 - 2\log|1-2^{-\varepsilon}| + 2\log 2}{2\log(3+\sqrt{8})} \\ &= \underbrace{\frac{\pi/2}{\log(3+\sqrt{8})}}_{:=D_1^{(1)}} t + \underbrace{\frac{\log 10}{\log(3+\sqrt{8})}}_{:=D_2^{(1)}} d + \underbrace{\frac{\log 2 - \log(1-2^{-\varepsilon})}{\log(3+\sqrt{8})}}_{D_\varepsilon^{(1)}}, \end{aligned} \tag{17}$$

thus concluding the proof. The deduction for BLC-series is analogical. □

Corollary 1. *Under the conditions of Theorem 1, for $\varepsilon = 10^{-m}$, $m \in \mathbb{N}$, the series (1) to compute the Riemann zeta-function with d decimal digits of accuracy, requires the number of terms*

$$n^{(j)} = \left\lceil D_1^{(j)} t + D_2^{(j)}(d+m) \right\rceil + 2 - j. \tag{18}$$

Proof of Corollary 1. The result (18) follows immediately, if we notice that for $\varepsilon \to 0$ we have

$$\log(1 - 2^{-\varepsilon}) = \log \varepsilon + \log\log 2 + o(1).$$

□

2.4. NA-Modifications of MB- and BLC-Algorithms

Limit theorems for coefficients of MB- and BLC-series enable us to derive a normal approximation for coefficients $\psi_{n,k}^{(j)}$ (cf. (24) in [3]). We can formulate the following theorem.

Theorem 2. *Coefficients $\psi_{n,k}^{(j)}$ of the series (1) satisfy*

$$\psi_{n,k}^{(j)} = 1 - \Phi\left(\frac{k - \mu_n^{(j)}}{\sigma_n^{(j)}}\right) + O\left(\frac{1}{\sqrt{n}}\right). \tag{19}$$

Coefficients $\mu_n^{(j)}$ and $\sigma_n^{(j)}$ are presented in Table 2.

Table 2. Coefficients of the expression (19).

j	$\mu_n^{(j)}$	$\sigma_n^{(j)}$
1	$\frac{n}{\sqrt{2}}$	$\frac{\sqrt{n}}{\sqrt[4]{32}}$
2	$\frac{n}{2}$	$\frac{\sqrt{n}}{2}$

Proof of Theorem 2. Let us start with MB-series coefficients. Suppose A_n is an integral random variable with the probability mass function

$$P(A_n = k) = \frac{u_{n,k}}{\sum_{j=0}^{n} u_{n,j}}, \quad k = 0, \ldots, n. \tag{20}$$

Here (cf. (1) in [3])

$$u_{n,k} = n\frac{(n+k-1)!4^k}{(n-k)!(2k)!}, \quad n \in \mathbb{N}, \ 0 \leqslant k \leqslant n. \tag{21}$$

Thus,

$$\psi_{n,k}^{(1)} = 1 - \frac{\sum_{j=0}^{k} u_{n,j}}{\sum_{j=0}^{n} u_{n,j}}. \tag{22}$$

Let $F_n(x)$ be the cumulative distribution function of the random variable A_n (20), then (cf. Theorem 3 in [7])

$$F_n(\sigma_n^{(1)} x + \mu_n^{(1)}) = \Phi(x) + O\left(\frac{1}{\sqrt{n}}\right), \qquad x \in \mathbb{R}. \tag{23}$$

Note that the cumulative distribution function

$$F_n\left(\sigma_n^{(1)}x + \mu_n^{(1)}\right) = \sum_{j \leqslant \sigma_n^{(1)}x + \mu_n^{(1)}} \frac{u_{nj}}{\sum_{j=0}^{n} u_{nj}}.$$

Denoting $k = \lfloor \sigma_n x + \mu_n \rfloor$ and taking into account (22) and (23), we obtain

$$1 - \psi_{n,k}^{(1)} = \Phi\left(\frac{k - \mu_n^{(1)}}{\sigma_n^{(1)}}\right) + O\left(\frac{1}{\sqrt{n}}\right).$$

The first part of the theorem follows. Similar result for BLC-coefficients $\psi_{n,k}^{(2)}$ has been proven in [2]. □

Theorem 2 allows us to choose the number of terms $n^{(j)}$ for the series (1),

$$n^{(j)} = \lceil \mu_n^{(j)} + z_d \sigma_n^{(j)} \rceil, \tag{24}$$

for n large enough. Here $z_d = \Phi^{-1}(1 - 10^{-d})$. Note that

$$n^{(1)} \sim \underbrace{\frac{\pi}{2\sqrt{2}\log(3+\sqrt{8})}}_{=0.630...} t, \qquad n^{(2)} \sim \underbrace{\frac{\pi}{4\log 2}}_{=1.133...} t,$$

for fixed σ and d. The refined version of NA-modification based methodology is summarized in Section 4.

2.5. Empirical Insights for NA-Modifications

While performing practical computations using NA-algorithms, we have noticed that the values produced were significantly more accurate than otherwise implied by d in the analytic estimate (10). In order to increase the performance and to have a clear course for future theoretical refinements, we propose empirical formulae for the minimum number of terms in the series (1) to compute the Riemann zeta-function with d decimal digits of accuracy.

Kuzma has proposed the following empirically-based estimate for the number of terms for the BLC-series ($d = 6$),

$$n^{(0)} = \lceil 0.67658827t + 113.26486067 \rceil. \tag{25}$$

In the present section, we offer an improvement to this estimate.

Figure 1 displays the minimum n required to calculate the Riemann zeta function with $d = 6$ digits of accuracy using NA- and BLC-algorithms at $\sigma = 1/2$, $t \in [1000, 1050]$ (the blue curve). The curves have clearly visible periodic peaks (marked by red vertical lines). The peaks have a period of $\lambda = 2\pi/\log 2$, which correspond τ_k special points of Theorem 1. Since we are interested in the upper bound of this empirical curve, for the following calculations we use the points $t = \lambda k$, $k \in \mathbb{N}$.

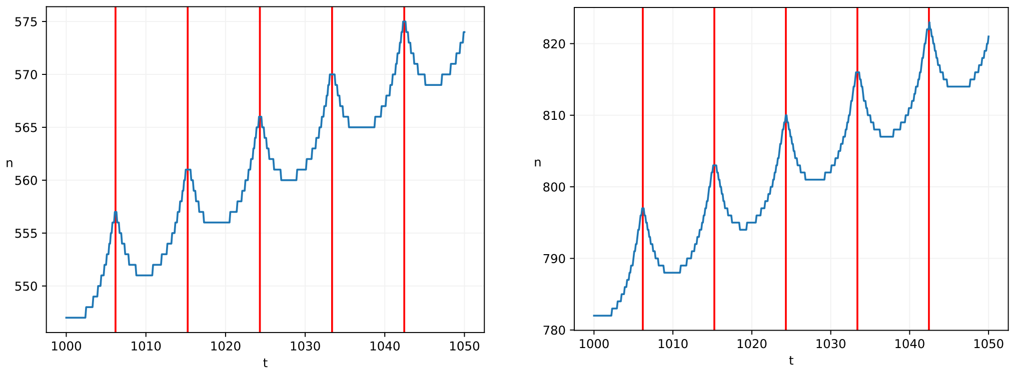

(**a**) NA-algorithm (**b**) BLC-algorithm

Figure 1. Periodic peaks of the minimum number of terms (the blue curves) in series (1) for $d = 6$ digits of accuracy at $(\sigma, t) \in 1/2 \times [1000, 1050]$. The curves have clearly visible periodic peaks, marked by red vertical lines.

Figure 2 shows regression models

$$n^{(j)} = \left\lceil a^{(j)} t + b^{(j)} \sqrt{t} + c^{(j)} \right\rceil \tag{26}$$

derived for $d \in [1, 10]$ using the points $(\sigma, t) \in 1/2 \times (0, 10{,}000)$. Each graph represents a fitted curve for a different d value.

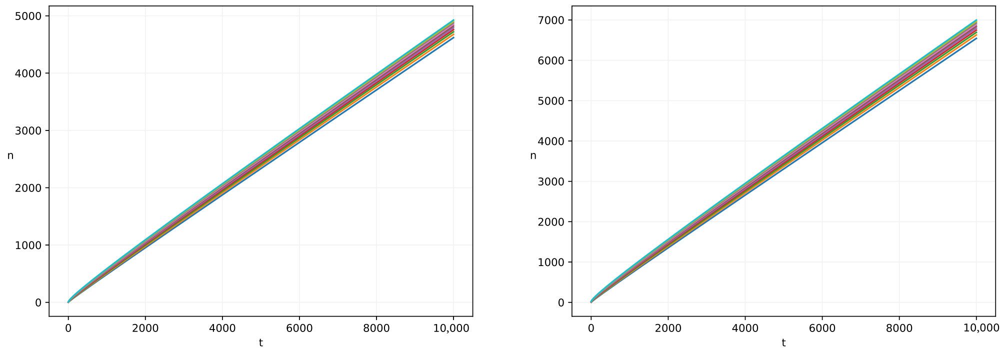

(**a**) NA-algorithm (**b**) BLC-algorithm

Figure 2. Regression models (26) for the minimum number of terms in series (1), derived for the accuracies $d \in [1, 10]$.

Figure 3 illustrates fluctuations of the coefficients of the regression models (26) by d. Here we can clearly see that $a^{(1)}$ has no correlation with d while $b^{(1)}$ and $c^{(1)}$ does.

Fitting $b^{(j)}$ with $b^{(j)} = x\sqrt{d} + y$ and $c^{(j)}$ with $c^{(1)} = xd + y$ we obtain the following coefficients for (26) (see Table 3):

Table 3. Coefficients of the regression model (26).

j	$a^{(j)}$	$b^{(j)}$	$c^{(j)}$
1	0.451	$1.407\sqrt{d} - 0.245$	$0.371d + 0.195$
2	0.637	$2.026\sqrt{d} - 0.272$	$1.602d - 0.026$

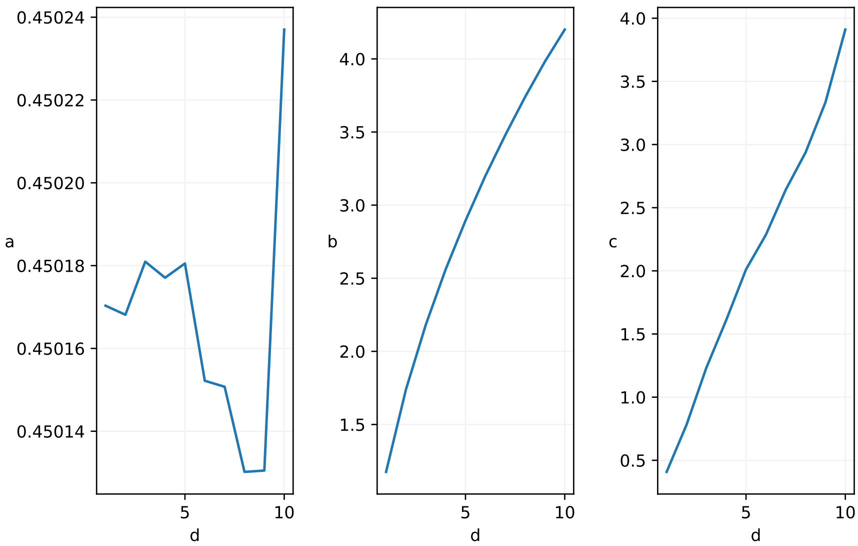

Figure 3. Coefficients of the regression models $a^{(1)}$, $b^{(1)}$ and $c^{(1)}$ plotted against the decimal digits of accuracy.

3. Visualizations of Fractal Structures Associated with the Riemann Zeta Function

3.1. Methods of the Visualization

In this study we employ two methods to reveal the Riemann zeta function underlying nature. The first heuristic method (FH-method) calculates RGB colors of the graph of the Riemann zeta function, using a composition of special functions. Suppose we have a function $f : (\mathbb{R}^+, \mathbb{C}) \to \mathbb{N}_0$:

$$f(x,z) = \begin{cases} \lfloor x \log |z| \rfloor, & \text{if} \quad z \neq 0, \\ 0, & \text{if} \quad z = 0. \end{cases} \tag{27}$$

Now we can define functions f_1, f_2, f_3:

$$f_1(x,z) = f(\eta_1, \zeta(s)), \quad f_2(x,z) = f(\eta_2, \Re(\zeta(s))), \quad f_3(x,z) = f(\eta_3, \Im(\zeta(s))). \tag{28}$$

Next, we calculate (R, G, B) colors of each pixel of the graph of the Riemann zeta function using polynomial functions of f_k (see Table 4):

$$\begin{aligned} R &= g_1^{(l)}(f_1, f_2, f_3) \mod 256, \\ G &= g_2^{(l)}(f_1, f_2, f_3) \mod 256, \\ B &= g_3^{(l)}(f_1, f_2, f_3) \mod 256. \end{aligned}$$

Table 4. List of $g_k^{(l)}$ functions.

l	$g_1^{(l)}$	$g_2^{(l)}$	$g_3^{(l)}$
1	f_1	f_2	f_3
2	$255 - f_1 f_2 f_3$	$f_2 f_3$	$255 - f_2$
3	f_1	f_2	f_3^2
4	$f_1 f_3$	f_2	f_3
5	$f_1 f_3$	$f_2 f_3$	f_3

The second approach (second fractal heuristic (SFH) method) is based on the application of the Mandelbrot set to the visualization of the Riemann zeta function. Suppose we aim to visualize $\zeta(\sigma + it)$ for $(\sigma, t) \in (\sigma_1, \sigma_2) \times (t_1, t_2)$. First, we introduce the log-transformation for each point (x, y) of the graph,

$$\begin{cases} x = L(\Re(\zeta(\sigma + it))), \\ y = L(\Im(\zeta(\sigma + it))), \end{cases} \tag{29}$$

thus obtaining the set $Q = (x_{min}, y_{min}) \times (x_{max}, y_{max})$. Here

$$L(x) = \begin{cases} \log|x|, & \text{if } x \neq 0, \\ 0, & \text{if } x = 0. \end{cases} \tag{30}$$

Next, we linearly transform Q into the subset S of the complex plane,

$$(x, y) \in Q \to (x^*, y^*) \in S.$$

We take $S = (-2, 0.47) \times (-1.12i, 1.12i)$, where the Mandelbrot set is defined. Then we use an algorithm to generate the Mandelbrot set, setting the start position at $z_0 = 0$ and $z^* = (x^*, y^*)$:

$$z_{k+1} \leftarrow z_k^2 + z^*. \tag{31}$$

Suppose that $k \in \mathbb{N}$, $k \leqslant v_{max}$ indicates the number of iterations (31), required to ascertain that z^* does not belong to the Mandelbrot set, with

$$|z_{k+1}| \leqslant 2 \quad \text{and} \quad k < v_{max}.$$

For $k = v_{max}$, it is unclear if z^* does not belong to the Mandelbrot set. Now let $k_0 = \lfloor 50k \rfloor$. We calculate RGB color for the z^* point by the following rule:

$$RGB = \begin{cases} (0, \quad 0, \quad 0), & \text{if } k = v_{max}, \\ (255, \quad 255, \quad k_0 \mod 256), & \text{if } 510 < k_0 < v_{max}, \\ (100, \quad k_0 \mod 256, \quad 255), & \text{if } 255 < k_0 \leqslant 510, \\ (0, \quad 0, \quad k_0 \mod 256), & \text{if } k_0 \leqslant 255. \end{cases}$$

3.2. Visual Investigations

The first visualization (see Figure 4) reveals the underlying structures in the "center" $S_1 \subset \mathbb{C}$ of the Riemann zeta function, received by two different methods (the color visualization and the fractal visualization). Here $S_1 = (-20, 8) \times (-14, 14)$. Figure 4a is obtained using FH-method with color parameters $\eta_1 = 100$ and $\eta_2 = \eta_3 = 8$. The color transform $g_k^{(1)}$ is linear (see Table 4). Figure 4b is obtained using SFH-method. Note small bright fractal feature on the right-hand side, calling for in-depth investigation.

Figure 5 presents zoom-in frames of S_2 region for the Riemann zeta function. Here $S_2 = (-5, 6) \times (\beta, \alpha + \beta)$, with four shifted in β intervals (see Table 5 for the ranges). The frames were received using FH-method with color parameters $\eta_1 = 100$ and $\eta_2 = \eta_3 = 8$. The color transform $g_k^{(1)}$ is linear (see Table 4). Note nontrivial zeros of the Riemann zeta function (blue disks, marked with arrows in Figure 5a,b).

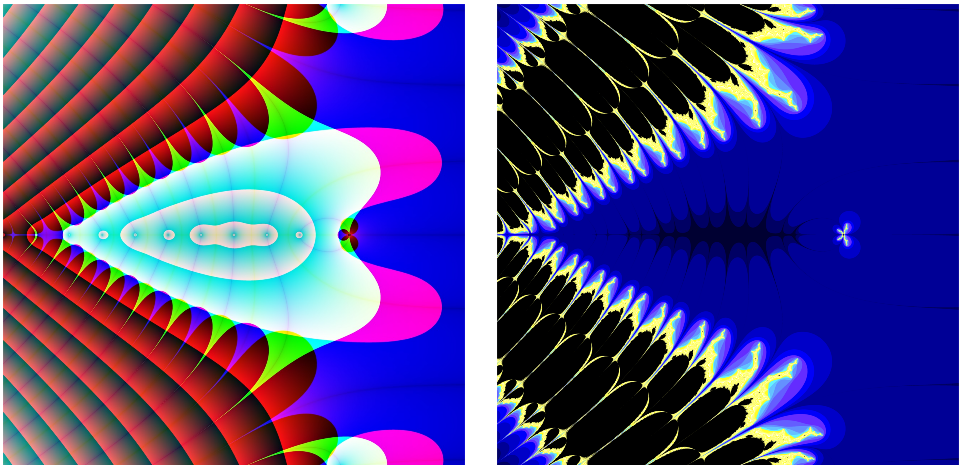

(**a**) Method 1: Color visualization (**b**) Method 2: Fractal visualization

Figure 4. The structures of the "center" of the Riemann zeta function, $(\sigma, t) \in (-20, 8) \times (-14, 14)$, received by SH and SFH methods. Note small fractal feature on the right-hand side of (**b**).

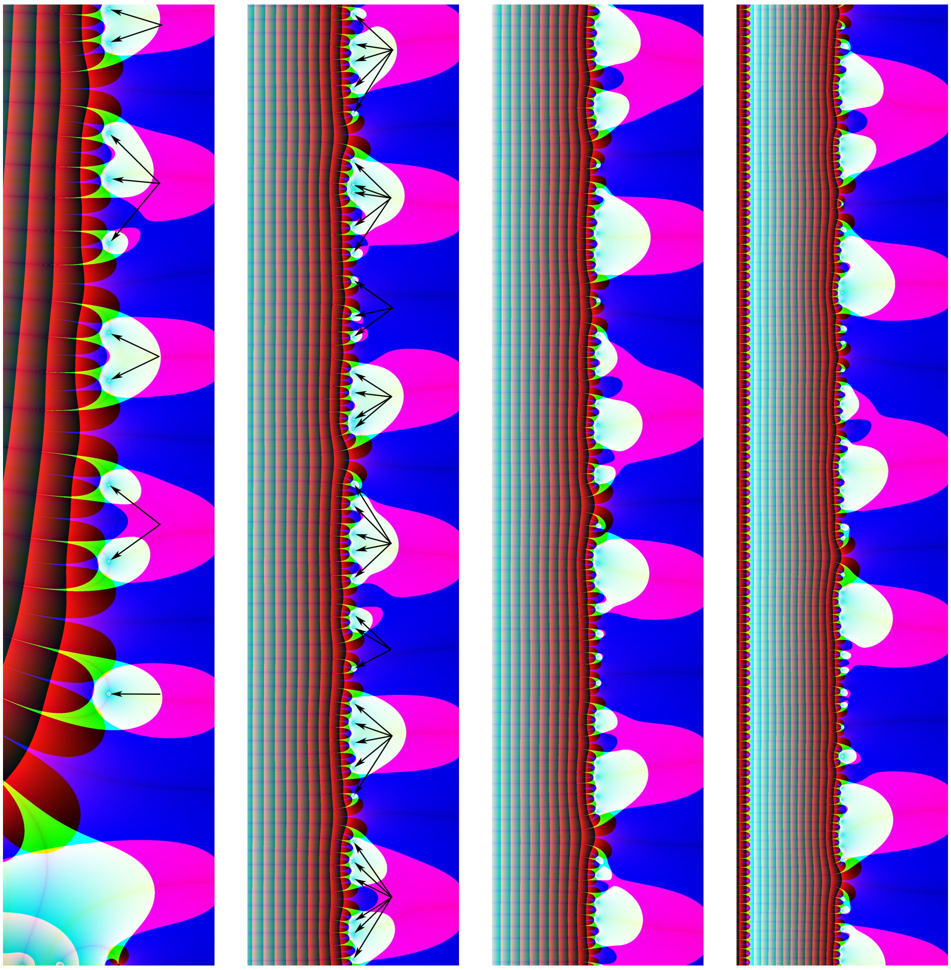

(**a**) (**b**) (**c**) (**d**)

Figure 5. FH-based zoomed-in frames of the Riemann zeta function (see Table 5 for the ranges). Note nontrivial zeros of the Riemann zeta function (blue disks, marked with arrows in Figure 5a,b).

Table 5. Ranges of the sets of Figure 5: $(\sigma, t) \in S_2$, $\alpha = 50$.

Figure	β	S_2
Figure 5a	0	$(-5, 6) \times (0, 50)$
Figure 5b	500	$(-5, 6) \times (500, 550)$
Figure 5c	1000	$(-5, 6) \times (1000, 1050)$
Figure 5d	5000	$(-5, 6) \times (5000, 5050)$

Figure 6 (obtained by SFH-method) extends the investigation of the fractal feature, associated with the Riemann zeta function, observed in Figure 4b. The frame Figure 6a represents zoomed-in image of the feature in the range $(0.2, 2.2) \times (-1.6, 1.6)$. The frame Figure 6b is the next magnification step, belonging to the range $(0.95, 1.05) \times (-0.08, 0.08)$. Fractal structures received in Figure 6b are examined further in Figure 7.

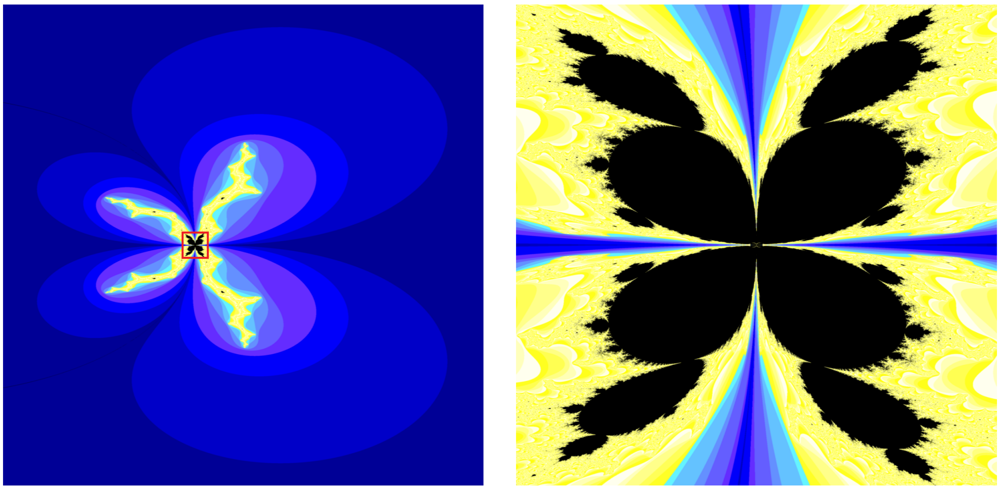

(**a**) (**b**)

Figure 6. Fractal features of the Riemann zeta function in the pole area (see Table 6 for the ranges). (**a**) gives zoomed-in image of the feature observed in Figure 4b. (**b**) represents the next magnification step (red rectangle).

Table 6. Ranges of the sets of Figure 6, $(\sigma, t) \in S_3$.

Figure	S_3
Figure 6a	$(0.20, 2.20) \times (-1.60, 1.60)$
Figure 6b	$(0.95, 1.05) \times (-0.08, 0.08)$

Figure 7a displays zoomed-in frame of the fractal border presented in Figure 6b. The next five frames (each of them corresponds to a colored rectangle in Figure 7a) uncover some aesthetically pleasing features of fractal structures associated with the Riemann zeta function. Note snowflake-shaped fractals in Figure 7c, as well as pinwheel-shaped ones in Figure 7d,e, resembling discs of spiral galaxies. Clockwise spinning Figure 7e reminds us of the grand design spiral galaxy NGC 4254 in Coma Berenices. Counter-clockwise rotating Figure 7d resembles the Pinwheel Galaxy NGC 5457 in Ursa Major. Invariant features of fractal geometry generated from images provide a good set of descriptive values for the recognition of regions and objects, e.g., fractal signatures of galaxies are examined with the aim of classifying them (cf. [16]). Figure 7 is received by SFH-method. The ranges of the sets are given in Table 7.

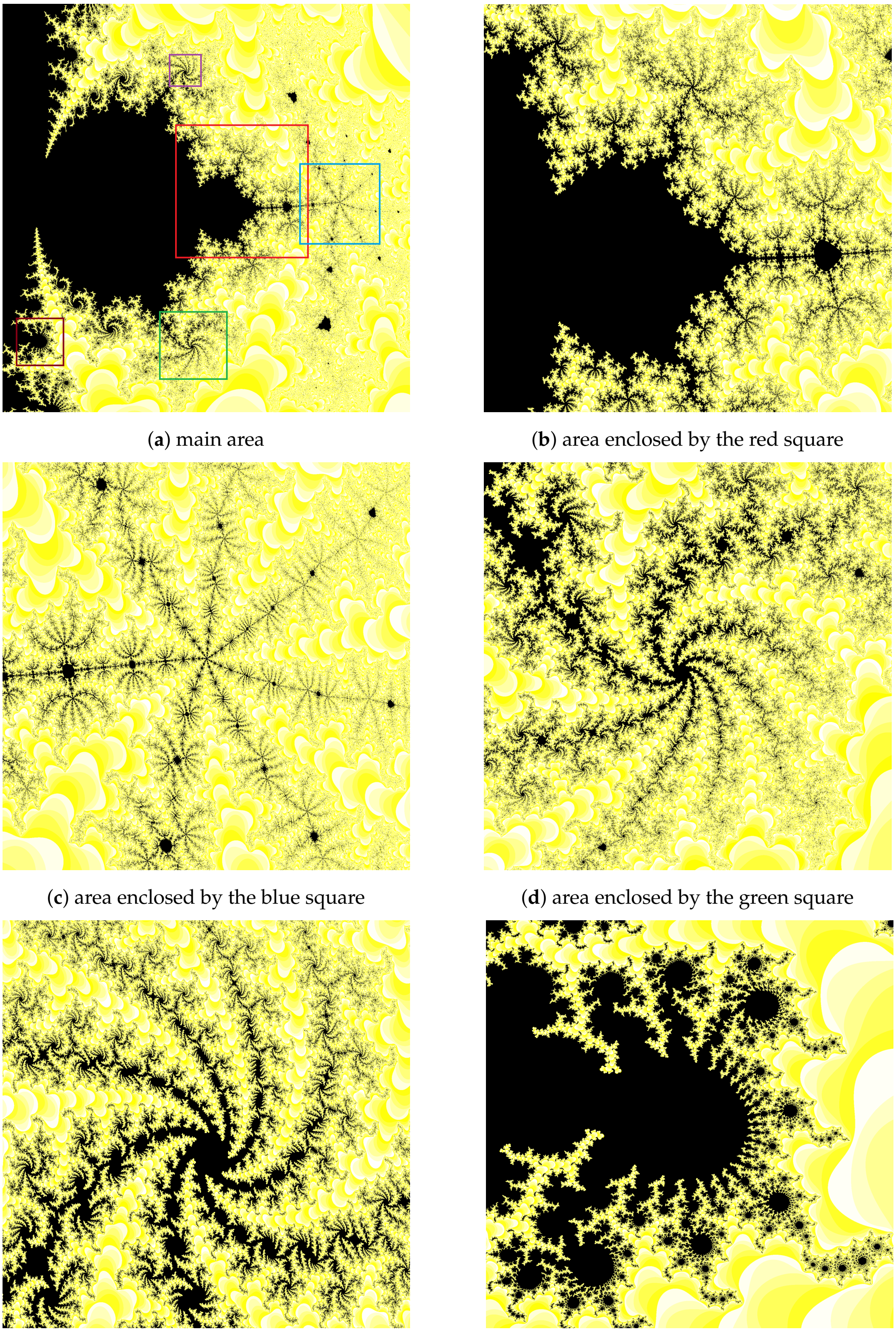

(a) main area

(b) area enclosed by the red square

(c) area enclosed by the blue square

(d) area enclosed by the green square

(e) area enclosed by the violet square

(f) area enclosed by the brown square

Figure 7. Fractal structures associated with the near-pole region of the Riemann zeta function. Frames (**b**–**f**) are zoomed-in rectangles of (**a**). Ranges of the sets are given in Table 7.

Table 7. Ranges of the frames of Figure 6.

Figure	σ_1	σ_2	t_1	t_2
Figure 7a	1.30000	1.04000	−0.034000	−0.024000
Figure 7b	1.03730	1.03925	−0.029875	−0.027925
Figure 7c	1.03730	1.03925	−0.029875	−0.027925
Figure 7d	1.03385	1.03550	−0.033200	−0.031550
Figure 7e	1.03410	1.03485	−0.026000	−0.025250
Figure 7f	1.03035	1.03150	−0.032850	−0.031700

Figure 8 illustrates other facets of the geography of the Riemann zeta function. Graphs for the range $(-30, 10) \times (-14, 16)$ are obtained using four different non-linear color transformations $g_k^{(l)}$, where $g_1^{(l)} \neq f_1$ or $g_2^{(l)} \neq f_3$ or $g_3^{(l)} \neq f_3$. Color parameters are given in Table 8.

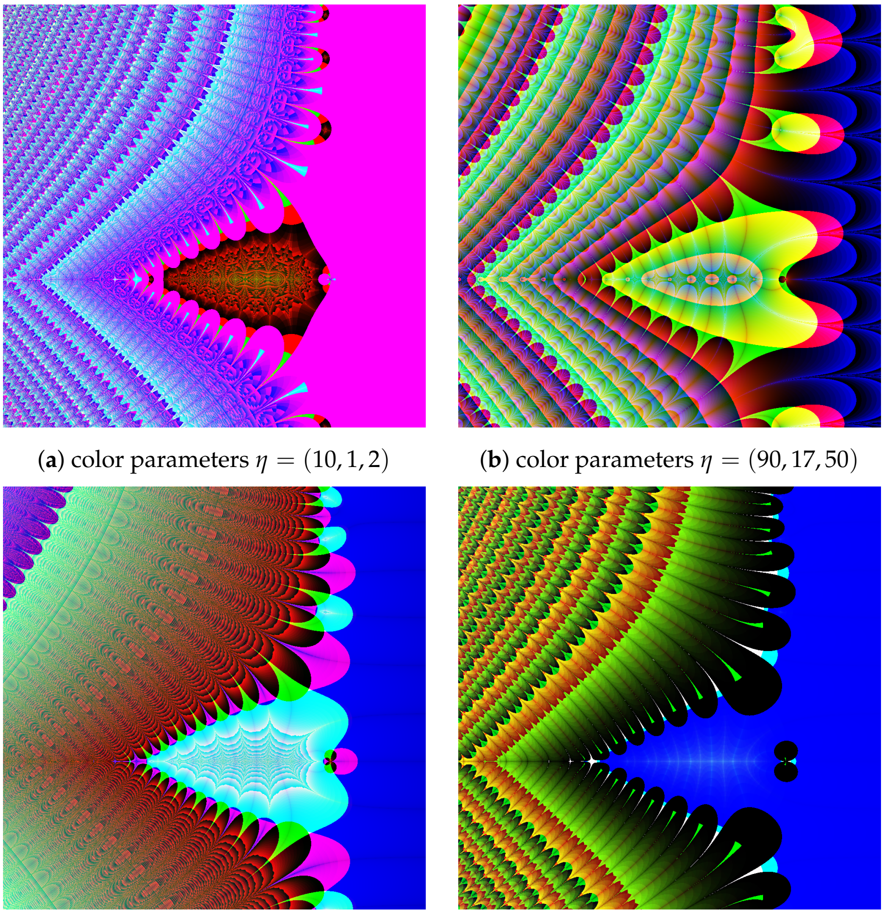

(**a**) color parameters $\eta = (10, 1, 2)$ (**b**) color parameters $\eta = (90, 17, 50)$

(**c**) color parameters $\eta = (9, 7, 5)$ (**d**) color parameters $\eta = (1, 2, 1)$

Figure 8. Four non-linear color maps of the Riemann zeta function for $(\sigma, t) \in (-30, 10) \times (-14, 16)$. Detailed color parameters are given in Table 8.

Table 8. Color parameters of Figure 8.

Figure	η_1	η_2	η_3	$g_k^{(l)}$
Figure 8a	10	1	2	$g_k^{(2)}$
Figure 8b	90	17	50	$g_k^{(3)}$
Figure 8c	9	7	5	$g_k^{(4)}$
Figure 8d	1	2	1	$g_k^{(5)}$

4. Computation and Visualization Algorithms

This section gives pseudocodes of the algorithms described in Sections 2 and 3.

4.1. Computation Algorithms

The first algorithm outlines MB- and BLC-approaches (cf. Theorem 1 and Corollary 1) with the corresponding empirical modifications (26) for the calculation of multiple values of the Riemann zeta functions while t is fixed.

The second algorithm outlines NA-modifications of MB- and BLC-methods. These approaches are more suitable for the calculation of specific values of the Riemann zeta function.

Results of numerical experiments with Algorithms 1 and 2 are presented in Section 5.

Algorithm 1 This algorithm will return multiple values of the Riemann zeta function for fixed t and array $\{\sigma_r\}$. Note that $L_k = \log k$ stand for precalculated logarithms.

procedure ZETA.M(σ : array $[1..N]$ of real numbers; d, m, j : natural numbers; t : real number) ▷ (see Table 9)

$$n \leftarrow \begin{cases} \left\lceil ((\pi/2)t + (d+m)L_{10})/\log(3+\sqrt{8}) \right\rceil + 1, & j = 1, \\ \left\lceil ((\pi/2)t + (d+m)L_{10})/L_2 \right\rceil, & j = 2, \\ \left\lceil a^{(j-4)}t + b^{(j-4)}\sqrt{t} + c^{(j-4)} \right\rceil, & j = 5 \text{ or } j = 6 \end{cases}$$

  if j is odd **then** ▷ MB^1- and EMB^5-block
    $T_0 \leftarrow -L_n, \quad l_{max} \leftarrow \lfloor n/\sqrt{2} \rfloor$
    for $l \in \{1..n\}$ **do**
      $T_l \leftarrow T_{l-1} + L_{n-l+1} + L_{n+l-1} - L_{2l-1} - L_{2l}$
    end for
    $H_0 \leftarrow \exp(T_0 - T_{l_{max}} - l_{max}L_4)$
    for $l \in \{1..n\}$ **do**
      $H_l \leftarrow H_{l-1} + \exp(T_l - T_{l_{max}} + (l - l_{max})L_4)$
    end for
    for $k \in \{0..n\}$ **do**
      $\psi_{n,k}^{(j)} \leftarrow (1 - H_k/H_n)(\cos(tL_{k+1}) - i\sin(tL_{k+1}))$
    end for
  else ▷ BLC^2- and $EBLC^6$ block
    for $k \in \{0..n\}$ **do**
      $\psi_{n,k}^{(j)} \leftarrow (\cos(tL_{k+1}) - i\sin(tL_{k+1}))\text{betainc}(k+1, n-k+1, 0.5)$
    end for
  end if
  $\lambda \leftarrow 2(\cos(tL_2) - i\sin(tL_2))$
  for $r \in \{1..N\}$ **do** ▷ Calculation of MB- or BLC-series for the corresponding σ_r
    $S \leftarrow 0, \quad p \leftarrow -1$
    for $k \in \{0..n\}$ **do**
      $p \leftarrow -p$
      $S \leftarrow S + p\psi_{n,k}^{(j)}\exp(-\sigma_r L_{k+1})$
    end for
    $S_r \leftarrow S/(1 - \lambda\exp(-\sigma_r L_2))$
  end for
return S ▷ Returns the array $S[1..N]$ of the Riemann zeta function values
end procedure

Algorithm 2 This algorithm will return values of the Riemann zeta function obtained by NA-modifications of MB- or BLC-method. Note that $L_k = \log k$ and $t > 10^3$.

```
function ZETA.NA(σ, t : real numbers; d, m, j : natural numbers)
    n ← (π/2)t + (d + m)L_10,    z ← Φ^{-1}(1 − 10^{-d})
    if j = 1 then                                                         ▷ NAMB-block
        n ← (n + L_2 − log L_2)/ log(3 + √8),    μ_n ← n/√2,    σ_n ← √n/ ⁴√32
    else                                                                  ▷ NABLC-block
        n ← (n − L_2 − log L_2)/L_2,    μ_n ← n/2,    σ_n ← √n/2
    end if
    k_0 ← ⌈μ_n + zσ_n⌉,    k_1 ← μ_n − zσ_n
    function ψ(n,k : nonnegative integers)
        if k < k_1 then
            ψ ← 1
        else
            ψ ← 1 − Φ((k − μ_n)/σ_n)
        end if
    end function
    S ← 0,    p ← −1
    for k ∈ {0..k_0} do
        p ← −p
        S ← S + pψ(n, k) exp(−σL_{k+1})(cos(tL_{k+1}) − i sin(tL_{k+1}))
    end for
return S/(1 − 2 exp(−σL_2)(cos(tL_2) − i sin(tL_2)))
end function
```

4.2. Visualization Algorithms

The third algorithm (Algorithm 3), corresponding the first heuristic method (FH-method), calculates RGB colors of the graph of the Riemann zeta function, using a composition of special functions.

Algorithm 3 This algorithm will return a colored image of Riemann zeta function for $(\sigma, t) \in (\sigma_{\min}, \sigma_{\max}) \times (t_{\min}, t_{\max})$. Other parameters: η_1, η_2, η_3—color parameters, g_1, g_2, g_3—polynomial functions of f_1, f_2, f_3 (see Table 4), w—width in pixels of output image img.

```
procedure FH(σ_min, σ_max, t_min, t_max, a, b, c : real numbers; w : natural number)
    h ← ⌊w · (t_max − t_min)/(σ_max − σ_min)⌋
    img ← [ ]
    for j ∈ {0..h − 1} do
        row ← [ ]
        t ← t_min + j · (t_max − t_min)/(h − 1)
        for k ∈ {0..w − 1} do
            σ ← σ_min + k · (σ_max − σ_min)/(w − 1)
            z ← ζ(σ + it)
            f_1 ← ⌊η_1 log |z|⌋
            f_2 ← ⌊η_2 log |ℜ(z)|⌋
            f_3 ← ⌊η_3 log |ℑ(z)|⌋
            g_1 ← g_1(f_1, f_2, f_3)
            g_2 ← g_2(f_1, f_2, f_3)
            g_3 ← g_3(f_1, f_2, f_3)
            RGB ← [g_1 mod 256, g_2 mod 256, g_3 mod 256]
            row ← row + RGB
        end for
        img ← img + row
    end for
end procedure
```

The fourth algorithm (Algorithm 4), corresponding the second fractal heuristic method (SFH-method), employs the Mandelbrot set to visualize the Riemann zeta function.

Algorithm 4 This algorithm will return fractalized image of Riemann zeta function for $(\sigma, t) \in (\sigma_{\min}, \sigma_{\max}) \times (t_{\min}, t_{\max})$. Here m stands for max iterations to get more precise fractal image, w - width in pixels of output image img. The output image utilizes yellow-black-blue color palette.

procedure SFH($\sigma_{\min}$, $\sigma_{\max}$, $t_{\min}$, $t_{\max}$: real numbers; w, m : natural numbers)
$h \leftarrow \lfloor w \cdot (t_{\max} - t_{\min})/(\sigma_{\max} - \sigma_{\min}) \rfloor$
$img \leftarrow [\,]$
$w_1 \leftarrow 2.47/(\sigma_{\max} - \sigma_{\min})$
$w_2 \leftarrow (0.47\sigma_{\min} + 2\sigma_{\max})/(\sigma_{\min} - \sigma_{\max})$
$w_3 \leftarrow 2.24/(t_{\max} - t_{\min})$
$w_4 \leftarrow 1.12(t_{\min} + t_{\max})/(t_{\min} - t_{\max})$
for $j \in \{0..h-1\}$ **do**
$row \leftarrow [\,]$
$t \leftarrow t_{\min} + j \cdot (t_{\max} - t_{\min})/(h-1)$
for $k \in \{0..w-1\}$ **do**
$\sigma \leftarrow \sigma_{\min} + k \cdot (\sigma_{\max} - \sigma_{\min})/(w-1)$
$z \leftarrow \zeta(\sigma + it)$
$z^* \leftarrow w_1 \mathrm{sign}(\Re(z)) \log|\Re(z)| + w_2 + (w_3 \mathrm{sign}(\Im(z)) \log|\Im(z)| + w_4)i$
$z \leftarrow 0$
$n \leftarrow 0$
while $|z| \leqslant 2$ **and** $n < m$ **do**
$z \leftarrow z^2 + z^*$
$n \leftarrow n + 1$
end while
$RGB \leftarrow [0,\ 0,\ 0]$
if $|z| > 2$ **then**
$l \leftarrow \lfloor 50n \rfloor$
if $l > 510$ **then**
$RGB \leftarrow [255,\ 255,\ l \mod 256]$
else if $l > 255$ **then**
$RGB \leftarrow [100,\ l \mod 256,\ 255]$
else
$RGB \leftarrow [0,\ 0,\ l \mod 256]$
end if
end if
$row \leftarrow row + RGB$
end for
$img \leftarrow img + row$
end for
end procedure

5. Numerical Experiments

We have performed numerical experiments with seven methods and modifications listed in Table 9.

Table 9. List of algorithms under examination.

j	Abbreviation	Algorithm
1	MB	modification of Borwein's efficient algorithm
2	BLC	series with binomial-like coefficients algorithm
3	$NAMB$	normal approximation-based modification of MB-algorithm
4	$NABLC$	normal approximation-based modification of BLC-algorithm
5	EMB	empirical modification of MB-algorithm
6	$EBLC$	empirical modification of BLC-algorithm
7	ZF	*Zetafast* algorithm

5.1. First Numerical Experiment

The first numerical experiment deals with normal approximation-based modifications (cf. Algorithm 2). Using $NAMB$ ($j = 3$), $NABLC$ ($j = 4$) and *Zetafast* ($j = 7$) methods we generate sequences of values of the Riemann zeta function $\{\zeta_{l,p}^{(j)}\}$, $1 \leqslant l \leqslant N$, $N = 10^5$, taking as arguments uniformly distributed $s_{l,p} \in S_p^{(1)}$. Here

$$S_p^{(1)} = \underbrace{(0.5, 1.5)}_{\sigma} \times \underbrace{(s_{k_p} + \rho_1, s_{k_{(p+1)}} - \rho_1)}_{t}, \tag{32}$$

where s_{k_p} stand for critical points (5) with $k_p = 2^{p+6}$, $1 \leqslant p \leqslant 3$, and $\rho_1 = 10^{-1}$. Thus we obtain 9 sequences overall (3 algorithms $\times$ 3 sets of arguments). Using *Zetafast* algorithm as a benchmark we calculate the accuracy $\delta_p^{(j)}$ and the relative performance $\theta_p^{(j)}$,

$$\delta_p^{(j)} = \max_{1 \leqslant l \leqslant N} \left| \zeta_{l,p}^{(j)} - \zeta_{l,p}^{(7)} \right|, \qquad \theta_p^{(j)} = \tau_p^{(j)} / \tau_p^{(7)}, \qquad 3 \leqslant j \leqslant 4, \tag{33}$$

where $\tau_p^{(j)}$ is the processing time of jth sequence $\{\zeta_{l,p}^{(j)}\}$, $1 \leqslant l \leqslant N$, for fixed p. The results of the first numerical experiment are presented in Table 10.

Table 10. Results of the first numerical experiment: accuracy $\delta_p^{(j)}$ and relative performance $\theta_p^{(j)}$, for $d = 6$, $m = 1$. The last line of the table shows the performance of ZF-algorithm (sec).

Method	j	$\mathbf{S_1^{(1)}}$	$\mathbf{S_2^{(1)}}$	$\mathbf{S_3^{(1)}}$
$NAMB$	3	1.80×10^{-11} 0.088	1.60×10^{-11} 0.12	2.90×10^{-11} 0.18
$NABLC$	4	1.82×10^{-11} 0.22	1.74×10^{-11} 0.32	3.35×10^{-11} 0.45
ZF	7	86.72	121.04	172.95

5.2. Second Numerical Experiment

The second numerical experiment aims to verify the accuracy of the algorithms on fixed horizontal lines, close to critical points. Using MB ($j = 1$) and BLC ($j = 2$) methods, their empirical modifications ($j = 5$ and $j = 6$) and *Zetafast* method ($j = 7$), we generate (cf. Algorithm 1) sequences of values of the Riemann zeta function $\{\zeta_{l,p}^{(j)}\}$, $1 \leqslant l \leqslant N$, $N = 10^5$, taking as arguments uniformly distributed $s_{l,p} \in S_p^{(2)}$. Here

$$S_p^{(2)} = \underbrace{(0.5, 1.5)}_{\sigma} \times t_p, \qquad t_p = s_{k_p} + \rho_1, \qquad k_p = 2^{p+6}, \qquad 1 \leqslant p \leqslant 3. \tag{34}$$

Thus we obtain 15 sequences overall (5 algorithms $\times$ 3 sets of arguments). Using the *Zetafast* algorithm as a benchmark we calculate the accuracy $\delta_p^{(j)}$ and the relative performance $\theta_p^{(j)}$ (cf. (33)). The results of the second numerical experiment are presented in Table 11.

The numerical experiments have been performed on Intel® Core™ i7-8750H 2.2 GHz (boosted to 4.0 GHz) processor with 16 GB DDR4 RAM. The code has been compiled with g++ 11.2.0 compiler using O3 optimization. C++ Boost library has been used for the implementation of the incomplete beta function for BLC-algorithm.

Table 11. Results of the second numerical experiment: accuracy $\delta_p^{(j)}$ and relative performance $\theta_p^{(j)}$ on fixed lines t_p, for $d = 6$, $m = 1$. The last line shows the performance of ZF-algorithm (sec).

Method	j	$S_1^{(2)}$	$S_2^{(2)}$	$S_3^{(2)}$
MB	1	1.68×10^{-11} 0.04	1.46×10^{-11} 0.055	2.65×10^{-11} 0.078
BLC	2	1.77×10^{-11} 0.1	1.55×10^{-11} 0.15	2.64×10^{-11} 0.2
EMB	5	6.43×10^{-7} 0.024	5.62×10^{-7} 0.032	5.51×10^{-7} 0.044
$EBLC$	6	7.07×10^{-7} 0.034	7.78×10^{-7} 0.048	7.84×10^{-7} 0.065
ZF	7	86.64	121.29	173.14

6. Discussion and Concluding Remarks

6.1. Discussion of the Results

We have refined the error terms and the expressions for the minimal number of terms in MB- and BLC-series of efficient algorithms for the computation of the Riemann zeta function, taking into account the behavior of the series in the neighborhoods of critical points. Theorem 1 shows that MB-based algorithms converge faster than BLC-based algorithms. Indeed, the MB-coefficient of the error term $\Theta_n^{(1)} = O(0.172^n)$ while $\Theta_n^{(2)} = O(0.5^n)$ (cf. (9)). However, BLC-approach has its advantages that might be useful in analytical research (cf. (4)). Note that this deficiency of the MB-algorithm is solved by the introduction of NA-modification (19).

The results of the numerical experiments (see Tables 10 and 11) show that MB and BLC methods, along with their normal and empirical modifications, allow fast and accurate calculations of the Riemann zeta function for large values of argument t. The results demonstrate that the introduced modifications accelerate computations of the Riemann zeta function, compared to *Zetafast* method. These versions of algorithms are well-suited for distributed computations and grid computing.

6.2. Findings of Visual Investigations of Fractal Structures, Associated with the Riemann Zeta Function

The illustrations obtained using FH-method clearly show the arrangement of trivial and non-trivial zeros of the Riemann zeta function in the complex plane (see Figure 5a,b). In addition to these points, we can also see dark 2D curves that satisfy the conditions $\Re(\zeta(\sigma + it)) = 0$ and $\Im(\zeta(\sigma + it)) = 0$ (see Figure 4a). The SFH-method distributes deformed copies of the Mandelbrot set in the complex plane, thus relating the values of the Riemann zeta function to the fractal structure. This allows for a visual assessment of essential changes in the Riemann zeta function values. Next, SFH-approach reveals notable symmetric fractals characterizing the neighborhood of the pole of the Riemann zeta function (see Figures 6 and 7).

6.3. Future Research Directions

Numerical experiments with empirical formulas indicate that the theoretical selection of the number of terms of the series n can be reduced. Next, the accuracy of the normal approximation-based modifications of MB and BLC algorithms might be refined by employing the theory of large deviations. The figures presented in this work reveal areas of the complex plane where the modulus of the Riemann zeta function exhibits very volatile values. This allows us to investigate the complex plane regions of $\Re\zeta(s) = \Im\zeta(s)$, thus enabling us to locate non-trivial zeros' positions visually. In future works, these visual instruments could be refined.

Author Contributions: Conceptualization, I.B., M.S. and L.K.; methodology, I.B. and M.S.; software, M.S. and L.K.; validation, I.B., M.S. and L.K.; formal analysis, I.B.; investigation, I.B., M.S. and L.K.; resources, M.S. and L.K.; writing—original draft preparation, I.B., M.S. and L.K.; writing—review and editing, I.B.; visualization, M.S. and L.K.; supervision, I.B. All authors have read and agreed to the published version of the manuscript.

Funding: This research received no external funding.

Institutional Review Board Statement: Not applicable.

Informed Consent Statement: Not applicable.

Data Availability Statement: Not applicable.

Acknowledgments: The authors would like to thank the anonymous reviewers for the careful reading of the manuscript and for providing constructive comments and suggestions, which have helped improve the paper's quality.

Conflicts of Interest: The authors declare no conflict of interest.

Abbreviations

The following abbreviations are used in this manuscript:

MB	Modification of Borwein's algorithm
BLC	Binomial-like coefficients
NA	Normal approximation
FH	First heuristic
SFH	Second fractal heuristic
NGC	New General Catalogue of Nebulae and Clusters of Stars

References

1. Borwein, P. An efficient algorithm for the Riemann zeta function. In *Constructive, Experimental, and Nonlinear Analysis*; Canadian Mathematical Society Conference Proceedings; Théra, M., Ed.; Americal Mathematical Society: Providence, RI, USA, 2000; Volume 27, pp. 29–34. Available online: http://www.cecm.sfu.ca/~pborwein/PAPERS/P155.pdf (accessed on 26 May 2022).
2. Belovas, I.; Sabaliauskas, M. Series with binomial-like coefficients for the evaluation and 3D visualization of zeta functions. *Informatica* **2020**, *31*, 659–680. https://doi.org/10.15388/20-INFOR434.
3. Belovas, I.; Sakalauskas, L.; Starikovičius, V. A method for accelerated computation of the Riemann zeta function on the complex plane. *Publ. Math.* **2022**, *100*, 167–184. https://doi.org/10.5486/PMD.2022.9120.
4. Šleževičienė, R. An efficient algorithm for computing Dirichlet L-functions. *Integral Transform. Spec. Funct.* **2004**, *15*, 513–522, https://doi.org/10.1080/1065246042000272072.
5. Vepštas, L. An efficient algorithm for accelerating the convergence of oscillatory series, useful for computing the polylogarithm and Hurwitz zeta functions. *Numer. Algorithms* **2008**, *47*, 211–252. https://doi.org/10.1007/s11075-007-9153-8.
6. Coffey, M.W. An efficient algorithm for the Hurwitz zeta and related functions. *J. Comput. Appl. Math.* **2009**, *225*, 338–346. https://doi.org/10.1016/j.cam.2008.07.040.
7. Belovas, I. Series with binomial-like coefficients for the Riemann zeta function. *Ann. Mat. Pura Appl.* **2022**, *201*, 903–912. https://doi.org/10.1007/s10231-021-01142-1.
8. King, C. Fractal geography of the Riemann zeta function: Part I. *Prespacetime J.* **2012**, *3*, 319–340. Available online: https://prespacetime.com/index.php/pst/article/view/357/352 (accessed on 26 May 2022).
9. Woon, S.C. Fractals of the Julia and Mandelbrot sets of the Riemann Zeta Function. *arXiv* **1998**, https://doi.org/10.48550/arXiv.chao-dyn/9812031.

10. Tingen, L.L. The Julia and Mandelbrot Sets for the Hurwitz Zeta Function. Master's Thesis, University of North Carolina Wilmington, Wilmington, NC, USA, 2009. Available online: http://dl.uncw.edu/Etd/2009-3/tingenl/larrytingen.pdf (accessed on 26 May 2022).
11. Blankers, V.; Rendfrey, T.; Shukert, A.; Shipman, P.D. Julia and Mandelbrot sets for dynamics over the hyperbolic numbers. *Fractal Fract.* **2019**, *3*, 6. https://doi.org/10.3390/fractalfract3010006.
12. Fischer, K. The Zetafast algorithm for computing zeta functions. *arXiv* **2017**, arXiv:1703.01414.
13. Borwein, P.; Choi, S.; Rooney, B.; Weirathmueller, A. *The Riemann Hypothesis: A Resource for the Afficionado and Virtuoso Alike*; Springer: New York, NY, USA, 2008. https://doi.org/10.1007/978-0-387-72126-2.
14. Laurinčikas, A. *Limit Theorems for the Riemann Zeta-Function*; Springer: Dordrecht, The Netherlands, 1996; ISBN 978-94-017-2091-5.
15. Gradshteyn, I.S.; Ryzhik, I.M. *Table of Integrals, Series, and Products*, 8th ed.; Academic Press: Cambridge, MA, USA, 2014.
16. Lekshmi, S.; Revathy, K.; Prabhakaran Nayar, S.R. Galaxy classification using fractal signature. *Astron. Astrophys.* **2003**, *405*, 1163–1167. https://doi.org/10.1051/0004-6361:20030541.